We are IntechOpen, the world's leading publisher of Open Access books Built by scientists, for scientists

4,800
Open access books available

122,000
International authors and editors

135M
Downloads

Our authors are among the

154
Countries delivered to

TOP 1%
most cited scientists

12.2%
Contributors from top 500 universities

CLARIVATE ANALYTICS BOOK CITATION INDEX INDEXED

WEB OF SCIENCE™

Selection of our books indexed in the Book Citation Index in Web of Science™ Core Collection (BKCI)

Interested in publishing with us?
Contact book.department@intechopen.com

Numbers displayed above are based on latest data collected.
For more information visit www.intechopen.com

Chapter 9

Aluminum- and Iron-Doped Zinc Oxide Nanorod Arrays for Humidity Sensor Applications

Ahmad Syakirin Ismail, Mohamad Hafiz Mamat and Mohamad Rusop Mahmood

Additional information is available at the end of the chapter

http://dx.doi.org/10.5772/67661

Abstract

Metal-doped zinc oxide (ZnO) nanorod arrays have attracted much attention due to improvement in their electrical, structural, and optical properties upon doping. In this chapter, we discuss the effects of aluminum (Al)- and iron (Fe)-doping on ZnO nanorod arrays properties particularly for humidity sensor applications. Compared to Fe, Al shows more promising characteristics as doping element for ZnO nanorod arrays. The Al-doped ZnO nanorod arrays showed dense arrays, small nanorods diameter, and high porous surface. The I-V characteristics showed that Al-doped sample possesses higher conductivity. From the humidity sensing performance of the samples, Al-doped ZnO nanorod arrays possess the superior sensitivity, more than two times higher than that of the undoped ZnO nanorod arrays sample, demonstrating great potential of Al-doped ZnO nanorod arrays in humidity sensor applications.

Keywords: ZnO, Al-doped, Fe-doped, nanorod arrays, humidity sensors

1. Introduction

Zinc oxide (ZnO) has been the subject of extensive investigations for many decades. A stable hexagonal wurtzite structure of ZnO consists of tetrahedrally coordinated four –O or four –Zn atoms, having lattice constant of a = 3.25 Å and *c* = 5.2 Å with ratio *c*/a = ~1.60 close to ideal hexagonal cell (1.633) [1]. **Figure 1** shows the ball and stick illustration of the hexagonal wurtzite structure of ZnO [1]. The ZnO structure does not have the center of symmetry.

ZnO is abundantly available in nature as a mineral zincite, although most of the commercial ZnO samples are prepared through synthetic approaches. Owing to its interesting properties,

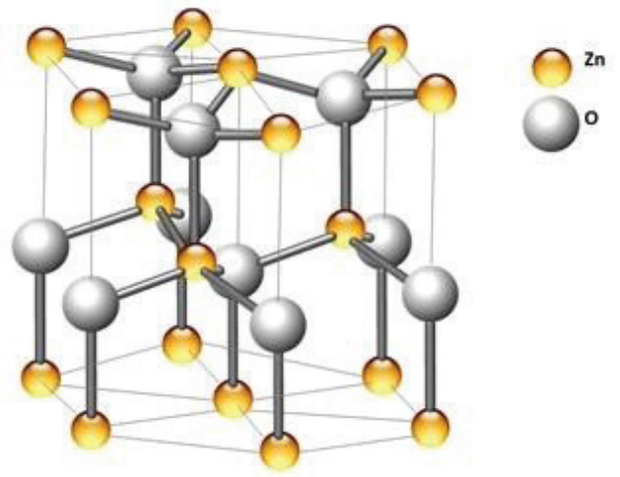

Figure 1. The illustration of the hexagonal wurtzite structure of ZnO.

such as a wide energy band gap of 3.37 eV, large exciton binding energy of 60 meV, good chemical and thermal stabilities, non-toxicity, and high transparency [2–5], ZnO has been applied in various applications such as textiles [6], medicines [7, 8], optoelectronic devices [9], solar cells [10, 11], and sensors [12, 13]. Other promising aspect of ZnO includes its ease of fabrication leading to generation of various kinds of nanostructures such as nanorods [14], nanowires [15], nanoflowers [16], and nanospheres [17]. Among them, one-dimensional (1-D) nanostructures (i.e., nanorods and nanowires) are more favorable in humidity sensor applications due to a higher surface-to-volume ratio, providing direct charge transport along the ZnO arrays and reducing the electron-hole pair recombination possibilities [18, 19]. These characteristics are crucial in fabricating high-performance humidity sensors. The performance of humidity sensor can be enhanced by introducing impurities to ZnO crystal through the doping process. As reported in previous studies, the doping process is capable of altering electrical conductivity, photocatalytic activity, and magnetic properties of ZnO [20–23]. In this chapter, we discuss recent developments in metal-doped ZnO, particularly in relation to the advantages of nanostructure-based humidity sensors. The preparation of Al- and Fe-doped ZnO nanorod array-based humidity sensors using the sol-gel immersion method is also included here followed by characterization of the structural, optical, and electrical properties of the fabricated humidity sensors.

2. Metal-doped ZnO

Doping is a process of introducing extrinsic elements into intrinsic structure for the purpose of improving and altering their basic properties such as structural, optical, and electrical. This process is crucial for various materials especially semiconductors since intrinsic semiconductor is known to possess deficiencies such as low carrier concentrations and lagging change in resistance values for humidity sensing applications [24, 25]. From the literature, ZnO was reported to be doped with numerous kinds of elements [26–29]. For instance, Kim et al. reported on the

http://dx.doi.org/10.5772/67661

fabrication of yttrium (Y)-doped ZnO nanorod arrays quantum dot (QD) synthesized solar cell using the chemical bath deposition method [30]. Due to Y-doping, the nanorod diameters were significantly reduced. In addition, the absorption coefficients of the films also improved after doping due to higher QD deposition. The conductivity of the film was improved when the concentration of doping was 50 mM. They also observed that the undoped ZnO nanorod arrays possess poor solar cell characteristics than that of the 50 mM Y-doped ZnO nanorod arrays sample. The substitution of the Y atom in ZnO lattice was expected to affect the transport properties of electrons by blocking the recombination process and increased the carrier concentration.

In another work, Kim et al. studied the fabrication of hydrophobic Al-doped ZnO nanorod arrays solar cell using the hydrothermal method [31]. In this study, they varied the concentration of Al dopant and controlled the growth period. The average diameters were significantly reduced when doped with Al. In addition, they reported that the undoped sample has higher hysteresis than that of Al-doped samples and the Al-doped ZnO nanorod arrays have a high self-cleaning performance. Meshki et al. fabricated Fe-doped ZnO nanorod arrays for two kinds of drug detection, namely, sulfamethoxazole and sulfamethizole [32]. When the nanorods were doped with Fe, the crystallite size of the ZnO nanorod arrays film was slightly decreased. The Fe-doped ZnO nanorods acquired a larger surface area than undoped ZnO nanorods, which likely led to the enhancement of electron transfer to the electrode surface.

In other research, Anbia and Fard fabricated a cerium (Ce)-doped ZnO nanoporous thin film humidity sensor using the screen printed method [33], in which they reported changes in humidity-sensing performance with doping and different sintering temperature. From their research, the Ce-doped ZnO thin film acquired smaller diameter of nanoparticles with a high porous surface. They also found that the Ce-doped ZnO film has better sensitivity to humidity than that of the undoped ZnO film. Peng et al. fabricated manganese (Mn)-doped ZnO nanopowders for humidity sensing application [34]. Based on their study, the undoped ZnO nanopowders possess larger nanoparticles and have low porosity. Upon Mn doping, the nanoparticle size is reduced with higher porous surface. As the concentration of Mn increased, the sensitivity of the ZnO nanopowders to humidity also increased, clearly higher than the undoped ZnO powder. They expected such behavior to occur due to higher H^+ ion density on the ZnO nanopowders surface and also higher concentration of defects with associated with oxygen vacancies.

From the above summary of the reported results, it is evident that doping is essential and very important for improving the useful properties of pristine ZnO structure. The improvements such as reduced crystallite size (increase surface area), high-quality surface structure, better photoluminescence properties, lower surface resistance, and high concentration of free carrier enhance the efficiency of the ZnO-based devices.

3. ZnO nanostructure-based humidity sensors

Humidity sensors have an important function in various situations, such as in industrial processing, agriculture, and environmental control since an uncontrolled amount of humidity can

be quite damaging to certain materials and processes [35]. Humidity sensors can be based on different sensing techniques, such as resistive, capacitive, optics, field effect transistor (FET), quartz crystal microbalance (QCM), and surface acoustic wave (SAW) [36–40]. Resistive-type humidity sensors are often preferred since they are easy to fabricate, have low cost, and have reliable response [41]. ZnO nanostructures have been widely studied for humidity sensing applications since it is highly sensitive to humidity. For example, Hendi et al. investigated the effect of different concentrations of an Sn-doped ZnO-based QCM humidity sensor [42]. They found that the crystallite sizes decrease when doped with Sn and the performance of the QCM humidity sensor improved when doped with Sn. Zhao et al. [43] have fabricated gallium (Ga)-doped ZnO nanowires piezo-humidity sensor using hydrothermal method. At low concentration of doping, they reported that the nanowires possess a small average diameter and doping with Ga helped to increase the oxygen vacancies and generate more free carriers, which in turn changed the piezoelectric screening effect and improved the water molecules adsorption. These results showed that Ga-doped ZnO nanowires yielded higher response to humidity compared to undoped ZnO nanowires.

The nano-scale structure in ZnO is very important in humidity detection due to larger surface-to-volume ratio and chemically reactive surface. According to Hsu et al. [44], the nanostructured surface of ZnO consists of high concentrations of oxygen vacancies, which provides highly active sites for water molecules adsorption. In their study, they fabricated ZnO dandelion-like nanostructures using a two-step thermal oxidation method, reporting increment in oxygen vacancies as the deposition temperature increased, which in-turn led to enhancement of humidity sensitivity.

High surface area is one of key factors that determines the high performance of a humidity sensor. The basic mechanism of a humidity sensor involves water molecules getting attached to the ZnO surface following the Grotthuss chain reaction [45]:

$$2\,H_2O \rightarrow H_3O^+ + OH^- \tag{1}$$

$$H_3O^+ \rightarrow H_2O + H^+ \tag{2}$$

The source of charge carriers is from the protonic transfer (H^+) among hydronium ions (H_3O^+) which is known by the term proton hopping. A higher surface area offers more surface reactions between the sensing element and water molecules leading to a greater number of carriers. This behavior was observed by Hong et al. when preparing ZnO nanorod arrays on top of the gallium (Ga)-doped ZnO seed layer film through the hydrothermal method [46]. They suggested that the increment concentrations of Ga in the ZnO seed layer film increased the thickness but reduced the nanorod diameter, resulting in an increased surface area of the nanorod arrays film and hence higher sensitivity for humidity detection.

4. Synthesis of zinc oxide nanorod arrays

For the synthesis of ZnO nanorod array films, a number of approaches have been reported. For instance, Ye et al. synthesized the sodium (Na)-doped ZnO nanorods on silicon (Si)

http://dx.doi.org/10.5772/67661

substrate using the chemical vapor deposition method [14] and studied the effects of Na concentrations on the ZnO nanorod properties. The growth of ZnO nanorods was done at 1000°C and 1800 Pa of temperature and pressure, respectively. Based on their report, the synthesized nanorods have a small diameter but they are not well aligned. In the report by Li et al. [47], the nanorod film was prepared with different dopants (Ga and Indium (In)) using the hydrothermal method on top of the ZnO seed layer-coated glass substrate. The purpose of their study was to investigate the influence of hydrogen annealing on the structural and luminescence properties of the ZnO nanorods. Through the preparation process, the nanorods were grown on the substrate with poor orientation and not aligned. According to them, the roughness of nanorods surface was increased due to thermal decomposition of the unstable surface status of polar and nonpolar faces of the ZnO structure. In the work by Son et al [48], the chemical bath deposition method was used to study the effect of seed layer thickness which was sputtered on Si substrate to the nanorod growth. Their results showed that the nanorods grew in a nonuniform manner in that the thickness and diameters of the nanorods were not uniform. However, higher thickness of the seed layer film produced nanorod arrays with better uniformity and alignment on the substrate.

From a review of the above-cited examples, it is evident that an ideal preparation of high-quality nanorod arrays does not necessarily depend on high-applied temperature and pressure. Therefore, a simpler, lower cost, and low-energy consumption method would be preferable. In our study, the synthesis of Al- and Fe-doped ZnO nanorod arrays was accomplished using a simple sol-gel immersion method. The nanorod arrays were grown on top of glass substrate with Al-doped ZnO as a seeded catalyst layer. For the preparation of the ZnO seeded layer catalyst, 0.4 M zinc acetate dehydrate ($Zn(CH_3COO)_2 \cdot 2H_2O$; 99.5% purity; Aldrich) was used as a precursor, 0.4 M mono-ethanolamine (MEA, $H_2NCH_2CH_2OH$; 99.5% purity; Aldrich) as a stabilizer, 0.004 M aluminum nitrate nonahydrate ($Al(NO_3)_3.9H_2O$; 98% purity; Analar) was used as a dopant source and 2-methoxyethanol as the solvent. The materials were mixed and then stirred on a hot plate stirrer at 80°C for 3 h and then aged for 24 h at room temperature to obtain a homogeneous solution. The prepared solution was spin coated at 3000 rpm for 1 min. The samples with coated film were then heated at 150°C for 10 min to dry and annealed at 500°C for 1 h.

The major interest of this study is the effect of Al and Fe doping on the intrinsic properties of ZnO. For the preparation of an undoped, Al-, and Fe-doped ZnO nanorod array film, 0.1 M zinc nitrate hexahydrate ($Zn(NO_3)_2 \cdot 6H_2O$; 98.5% purity; Schmidt) was used as a precursor, 0.1 M hexamethylenetetramine (HMT, $C_6H_{12}N_4$; 99% purity; Aldrich) as a stabilizer, and 0.001 M of aluminum nitrate dehydrate ($Al(NO_3)_3 \cdot 9H_2O$; 98% purity; Analar) and 0.001 M iron (III) nitrate nonahydrate ($Fe(NO_3)_3 \cdot 9H_2O$; 98% purity; Merck) as dopant sources. The reagents were mixed and dissolved in 500 ml of deionized water and then sonicated at 50°C for 30 min before being stirred on a magnetic hot plate stirrer at room temperature for 3 h to age the solutions. After the ageing process, the solutions were poured in a Schott bottle placed with seed layer-coated glass substrates. The seed layer-coated glass substrates were immersed in a water bath immersion tank at 95°C for 2 h. Then, the sample was cleaned and heated at 150°C for 10 min before being annealed at 500°C for 1 h.

The configuration of doped and undoped ZnO nanorod array-based humidity sensors was completed by depositing gold (Au) metal contact using sputter coater on top of the samples as the electrode. The structural properties of the samples were characterized using field emission

scanning electron microscopy (FESEM; JEOL JSM-7600F) and X-ray diffraction measurement (XRD; PANalytical X'Pert PRO). The optical properties of the samples were tested using a ultraviolet-visible-near-infrared (UV-vis-NIR; Varian Cary 5000) spectrophotometer. The electrical properties of the samples were characterized using two-point probe current-voltage (I-V; Advantest R6243) measurement. The performance of the humidity sensor of the fabricated sensors was analyzed using a humidity sensor measurement system (ESPEC-SH261). The schematics of preparation of doped and undoped ZnO nanorod array-based humidity sensors are shown in **Figure 2**.

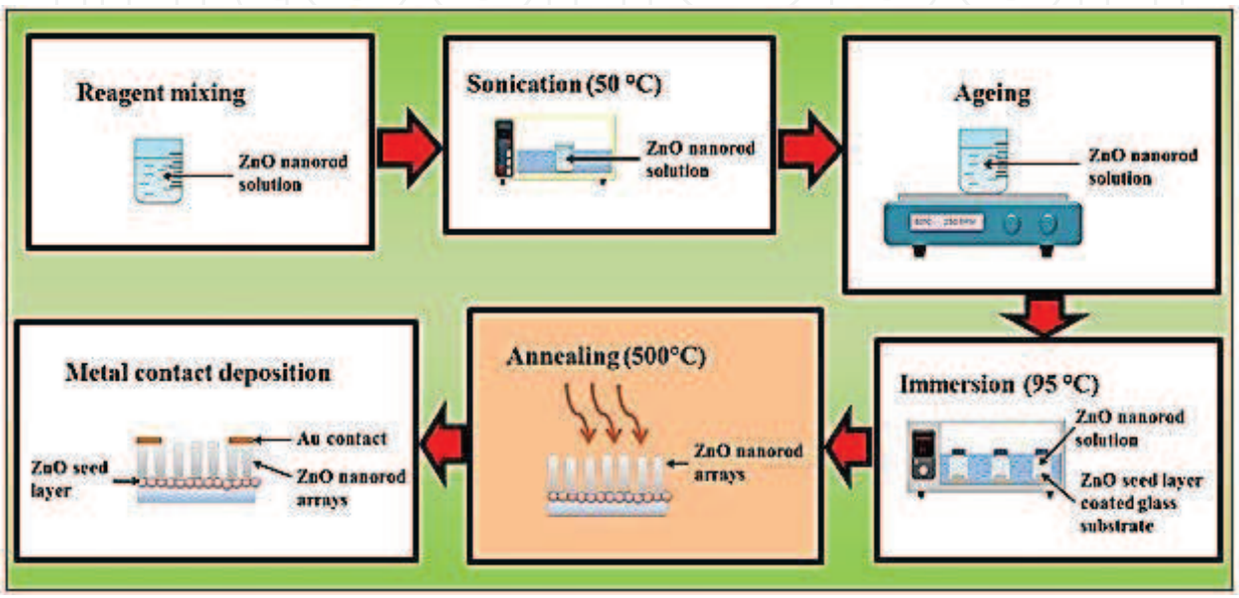

Figure 2. Schematics of the preparation of doped and undoped ZnO nanorod array-based humidity sensors.

5. Effects of aluminum and iron doping

The surface morphology, thickness, and the elemental analysis of the ZnO nanorod arrays were investigated using field emission electron scanning microscopy (FESEM) and energy-dispersive X-ray spectroscopy (EDS) as shown in **Figure 3**. **Figure 3(a–c)** shows the surface morphology of undoped and doped ZnO nanorod arrays taken at 30,000× magnification. It is observed that all samples produced have a hexagonal nanorod structure. The undoped sample has the largest average diameter of nanorod arrays of about 100 nm while Al- and Fe-doped ZnO-produced nanorod arrays have average diameters of 65 and 90 nm, respectively. Besides, the Al-doped ZnO nanorod array film is observed to possess higher porosity compared to undoped and Fe-doped samples. The reduction of nanorods size due to Al and Fe doping may be due to the smaller ionic radius of Al^{3+} (0.54 Å) and Fe^{3+} (0.64 Å) ions substituting the Zn^{2+} (0.74 Å) ion sites [49, 50]. The cross-sectional images of Al- and Fe-doped ZnO nanorod arrays are shown in **Figure 3(d–f)**. The thickness of undoped, Al-, and Fe-doped ZnO nanorod arrays films was estimated to be 1.1, 0.67, and 0.75 μm, respectively. A slight decrement in thickness of doped samples may be due to difference in the ionic radius as mentioned earlier. From

http://dx.doi.org/10.5772/67661

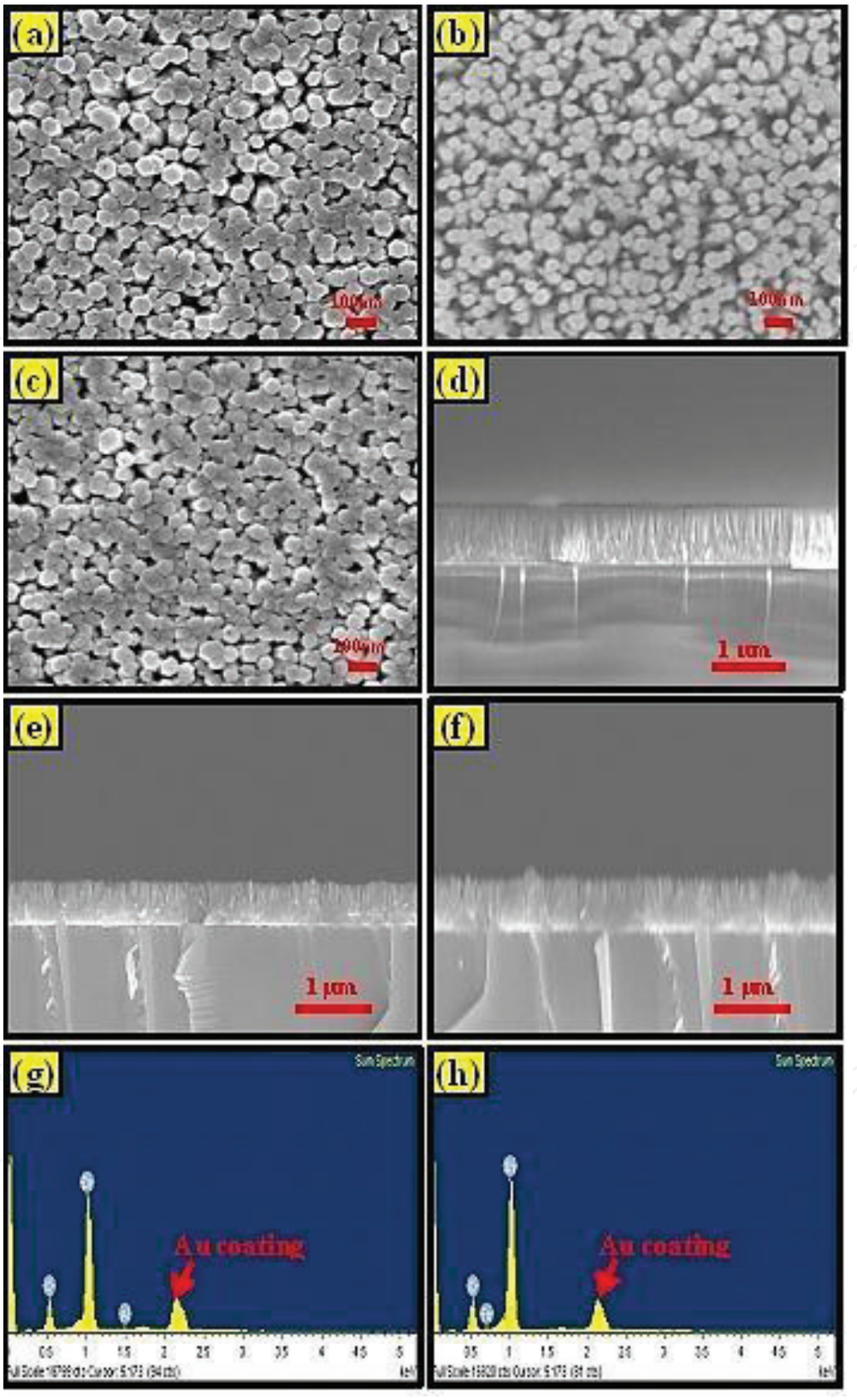

Figure 3. Surface morphology of (a) undoped, (b) Al-, and (c) Fe-doped ZnO nanorod array films that are prepared using sonicated sol-gel immersion. Cross-sectional images of (d) undoped, (e) Al-, and (f) Fe-doped ZnO nanorod array films. EDX spectrum of (g) Al- and (h) Fe-doped ZnO nanorod array films.

the EDS spectrum in **Figure 3(g** and **h)**, it is evident that the doping elements of Al and Fe appeared in each sample. The atomic ratio of Zn, Al, and O is expected to be 54.93:0.71:44.86, respectively, while the atomic ratio of Zn, Fe, and O is 53.60:0.21:46.18, respectively.

The XRD patterns of the undoped, Al-, and Fe-doped ZnO nanorod arrays for the 2θ range of 20–60° in **Figure 4** show the four main peaks with Miller indices of (100), (002), (101), and (102). The dominant (002) peak indicates that the growth is along *c*-axis orientation. In addition, it is also noticed that the diffraction peak at (002) orientation for doped samples is slightly decreased, which indicated that the doping elements are successfully substituting the ZnO structure. The degradation in peak intensities for doped samples was expected due to the difference in ionic radii of Al^{3+} and Fe^{3+} than that of Zn^{2+} ions. The position of the (002) peak for the undoped, Al-, and Fe-doped ZnO nanorod arrays occurs at 2θ = 34.38, 34.49, and 34.44°, respectively, which can be used to determine the lattice constant *c* using the following equation valid for hexagonal structure [51, 52]:

$$c = \frac{\lambda}{\sin\theta} \tag{3}$$

Here, λ = 1.54 Å is the X-ray wavelength of CuKα radiation. For the undoped, Al-, and Fe-doped ZnO nanorod arrays, *c* = 5.2108, 5.1947, and 5.2020 Å, respectively, was determined. The crystallite sizes, *D* of the undoped, Al-, and Fe-doped ZnO nanorod arrays, were calculated using the Scherrer formula [53]:

$$D = \frac{K\lambda}{\beta\cos\theta} \tag{4}$$

Here, *K* is a constant (0.94), and β is the full-width at half-maximum (FWHM) in radians. The (002) peak was used for the calculation of *D* for which the values of β of the undoped, Al-, and Fe-doped ZnO nanorod arrays are 0.2831, 0.3045, and 0.3037°, respectively. The *D* values of the undoped, Al-, and Fe-doped ZnO nanorod arrays were estimated to be 30.7, 28.5, and 28.6 nm, respectively. Thus, the values of *c* and *D* of the undoped ZnO nanorod arrays are lowered when doped with Al and Fe. According to Khuili et al. [54], lattice parameters *a* and *c* of Al-doped ZnO are smaller than those for undoped ZnO due to substitution of smaller Al^{3+} ions

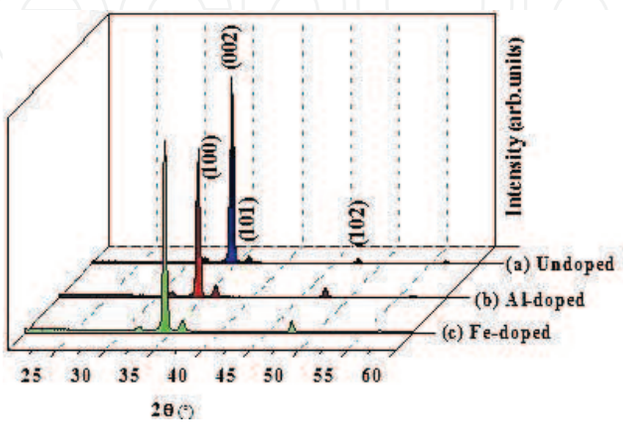

Figure 4. The XRD patterns of the undoped, Al-, and Fe-doped ZnO nanorod arrays.

http://dx.doi.org/10.5772/67661

into ZnO lattice, which is also confirmed by the simulated supercell structure. Yue et al. noted that the shrinkage of lattice constant and crystallite size when doped with Fe was due to the smaller ionic radius of Fe^{3+} compared to that of Zn^{2+} ions [50]. Bai et al. also found that the diffraction peak positions of ZnO have shifted to higher angles when doped with Fe, which might lead to reduction of lattice constant and crystallite size [55].

The optical properties of undoped and doped ZnO nanorod arrays were determined using UV-Vis-NIR spectrophotometer measurements between 350 and 800 nm at room temperature. **Figure 5** shows the transmittance properties of undoped, Al-, and Fe-doped ZnO nanorod arrays. The transmission decreases significantly at approximately 380 nm, which is attributed to the intrinsic ZnO band gap because of the direct transition of electrons between the edges of the valence band to the conduction band. From the spectra, average transmittances of undoped, Al-, and Fe-doped ZnO nanorod arrays were estimated to be 78.59, 76.96, and 75.10%, respectively. All doped samples exhibit a decrement in transmittance compared to the undoped sample. Previous studies reported that the transmittance decreased with Al and Fe doping [56, 57]. Such behavior occurred due to reduction of crystalline properties, which can be observed from the XRD data, and also due to enhancement of optical scattering by grain boundaries [57].

Figure 6 shows the I-V characteristics of undoped, Al-, and Fe-doped ZnO nanorod arrays. The I-V curves indicate that the nanorod arrays exhibit ohmic behavior, and the current increases with increasing voltage supplied for the nanorod arrays. The conductivity of the film, σ, was determined using the following equation [51]:

$$\sigma = \frac{1}{\rho}, \tag{5}$$

where ρ is the resistivity that can be expressed as

$$\rho = \left(\frac{V}{I}\right)\frac{wt}{l}, \tag{6}$$

where V is the supplied voltage, I is the measured current, t is the film's thickness, w is the electrode width, and l is the length between the electrodes. The active area of the thin films is

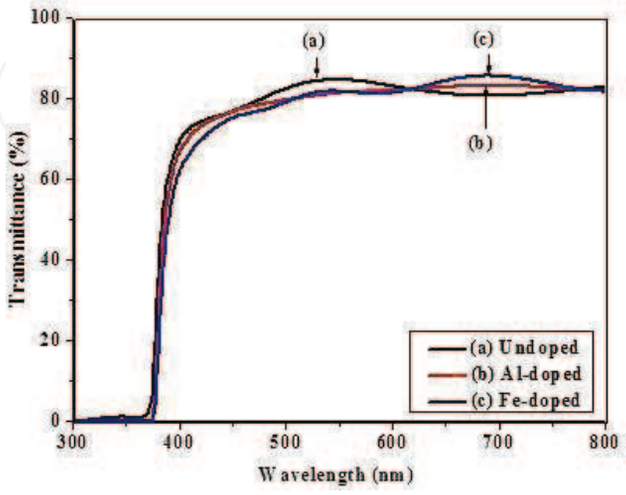

Figure 5. Transmittance properties of the undoped, Al-, and Fe-doped ZnO nanorod arrays.

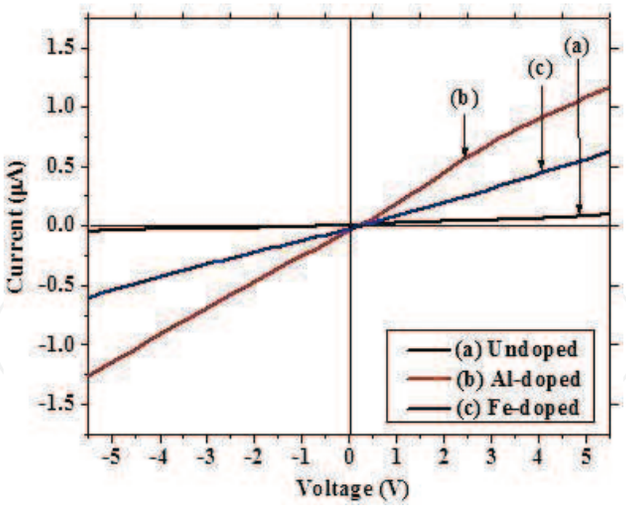

Figure 6. I-V plot for the undoped, Al-, and Fe-doped ZnO nanorod arrays.

3×10^{-6} m^2. The conductivity of undoped, Al-, and Fe-doped ZnO nanorod arrays is 0.08, 0.80, and 0.64 S cm^{-1}, respectively. It is observed that the conductivity of the nanorod array film significantly increased after doping. When ZnO was doped with Al^{3+} ions, the generation of free carriers is as follows [58]:

$$Al_2O_3 \rightarrow Al_{Zn\bullet} + 2O_o + \frac{1}{2}O_2 + 2e' \tag{7}$$

where $Al_{Zn}^{\bullet}$ represents one positive charge of Al that stayed in zinc lattice and act as donor. O_o is the oxygen ion in the inherent lattice. On the other hand, when ZnO was doped with Fe^{3+} ions, the generation of free carriers is as follows [55]:

$$Fe_2O_3 \rightarrow 2Fe_{Zn}^{\bullet} + 3O_o^x + 2e' \tag{8}$$

where $Fe_{Zn}^{\bullet}$ represents one positive charge of Fe that stayed in zinc lattice and act as donor. O_o is the oxygen ion in the inherent lattice while "x" represents the neutrality of O_o. Substitutions of two Fe atoms in the ZnO structure have induced two free electrons. This theory supports the enhancement of conductivity from Al- and Fe-doped samples compared to undoped ZnO nanorod arrays.

Humidity sensor responses of the prepared sensors in ambient with various RH (relative humidity) levels are shown in **Figure 7**. The measurements were conducted with 5 V DC-biased source at room temperature. During the adsorption process (40–90% RH), current signal increased steadily with increasing RH. On the other hand, during the desorption process (90–40% RH), current signal rapidly dropped until the signal recovers back to its initial current value. Response and recovery times are among the most imperative elements for evaluating the performance of humidity sensors. It is noted that the time taken by a sensor to achieve 90% of the total current change is defined as the response time in the case of adsorption or the recovery time in the case of desorption. The response/recovery times of the undoped, Al-doped, and Fe-doped ZnO nanorod arrays were measured to be 252/360, 270/90, and 243/108 s, respectively. Response and recovery behavior of sensor

http://dx.doi.org/10.5772/67661

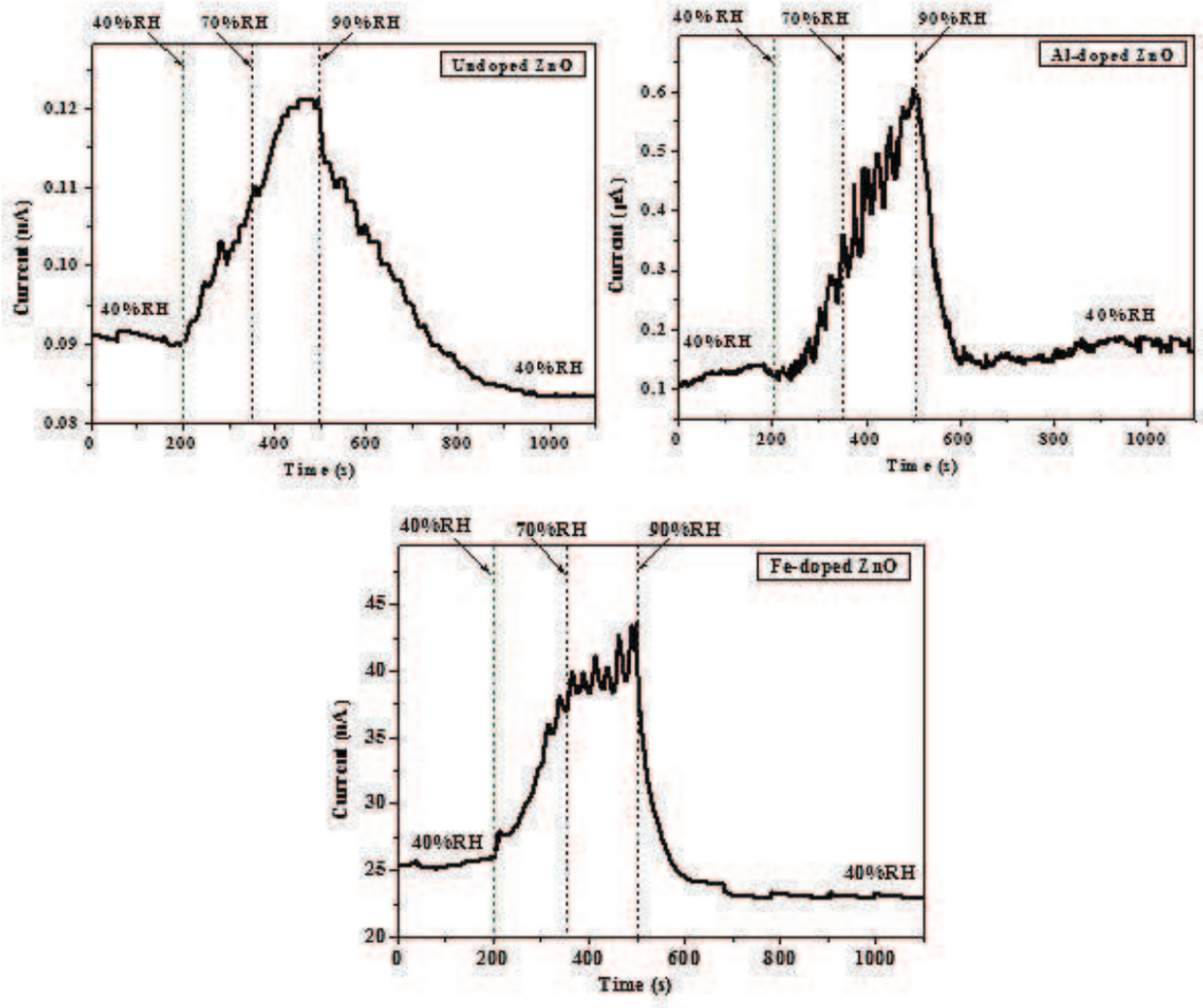

Figure 7. Humidity sensor response of (a) undoped, (b) Al- doped, and (c) Fe-doped ZnO nanorod array-based humidity sensors.

is dependent on large surface-to-volume ratio, where it helps to increase the adsorption of water molecules on the sensing element surface. Besides, with the availability of 1-D nanostructures (nanorod), it provides a large length-to-diameter ratio which can accelerate water molecules transfer to and from the interaction region as well as enhancing electron transfer along them [59].

Another important element of the humidity sensor is the sensitivity of the sensor. The sensitivity of undoped and doped ZnO nanorod array-based humidity sensors was estimated by using resistance data obtained from the response curve. Sensitivity was calculated by using the following relation [60, 61]:

$$S = \frac{R_a}{R_{\text{rh}}} \tag{9}$$

where S is sensitivity, R_a is the resistance of the sensor under exposure to the initial humidity level, and R_{rh} is the resistance of the sensor at the maximum humidity level. The values of

resistance were obtained using Ohm's law on the basis of a fixed bias voltage of 5 V, shown as follows:

$$V = IR \tag{10}$$

where V is the bias voltage, I is the measured current, and R is the resistance. The values of R_a/R_{rh} for undoped, Al-doped, and Fe-doped ZnO nanorod array-based humidity sensors were calculated to be $5.56 \times 10^9/4.17 \times 10^9$, $2.66 \times 10^7/8.33 \times 10^6$, and $2.08 \times 10^8\ \Omega/1.19 \times 10^8\ \Omega$, respectively. From R_a and R_{rh} values, the sensitivities of undoped, Al-doped, and Fe-doped ZnO nanorod array-based humidity sensors were calculated to be 1.33, 3.19, and 1.75, respectively. All doped samples show an improved performance in humidity sensing compared to the undoped sample. Zhu et al. also noticed the improvement of humidity sensing capabilities when they fabricated the piezoelectric-based ZnO nanowires humidity sensor [62]. In other report, Hendi et al. reported the response/recovery time of the ZnO-based QCM humidity sensor was improved when they doped ZnO with Sn [42]: this was attributed to easy diffusion of water molecules between ZnO nanopowders.

Zhu et al. reported that the doping process can increase the concentration of oxygen vacancies when the doping elements substituted the ZnO lattice which improved the performance of humidity sensor [62]. In addition, the substitution of Al^{3+} and Fe^{3+} ions has increased the charge density and offering more surface reaction with water molecules. This statement is supported by increase in conductivity and E_g values as discussed earlier. Furthermore, the superior performance of Al-doped ZnO nanorod arrays is likely related to the higher porosity of its surface as observed from FESEM image.

6. Concluding remarks

In this chapter, advantages of doping of zinc oxide (ZnO) nanostructures have been reviewed along with changes in their properties upon doping, particularly in relation to humidity sensing applications. Compared to Fe-doping, Al-doping shows more useful changes in properties for ZnO nanorod arrays for sensor applications. From the FESEM images, the Al-doped ZnO nanorods showed dense arrays with an average diameter of 65 nm, and higher porosity of the surface as compared to the Fe-doped sample which has an average diameter of 90 nm. No significant changes to the optical properties of doped samples were observed while the I-V characteristic of those doped samples possess a significant increment in conductivity compared to undoped ZnO nanorod arrays. Regarding the humidity-sensing performance of the samples, Al-doped ZnO nanorod arrays showed superior sensitivity, more than two times higher than that of the undoped ZnO nanorod array sample. These results show that Al-doped ZnO nanorod arrays has a promising future in humidity sensor applications.

Acknowledgements

This work was supported by the Fundamental Research Grant Scheme 600-RMI/FRGS 5/3 (57/2015) from the Ministry of Education Malaysia. The authors also would like to thank the Faculty of Electrical Engineering, NANO-ElecTronic Centre (NET), NANO-SciTech Centre

(NST), Research Management Centre (RMC) of UiTM and the Ministry of Higher Education of Malaysia for their funding, laboratory equipment, and support of this research.

Author details

Ahmad Syakirin Ismail[1*], Mohamad Hafiz Mamat[1,2] and Mohamad Rusop Mahmood[1,2]

*Address all correspondence to: kyrin_samaxi@yahoo.com

1 NANO-ElecTronic Centre (NET), Faculty of Electrical Engineering, Technology University Mara (UiTM), Shah Alam, Selangor, Malaysia

2 NANO-SciTech Centre (NET), Institute of Science (IOS), Technology University Mara (UiTM), Shah Alam, Selangor, Malaysia

References

[1] Özgür Ü, Alivov YI, Liu C, Teke A, Reshchikov MA, Doğan S, et al. A comprehensive review of ZnO materials and devices. Journal of Applied Physics. 2005;**98**:041301

[2] Al-Kuhaili MF, Durrani SMA, El-Said AS, Heller R. Enhancement of the refractive index of sputtered zinc oxide thin films through doping with Fe_2O_3. Journal of Alloys and Compounds. 2017;**690**:453-460

[3] Li C-C, Jhang J-H, Tsai H-Y, Huang Y-P. Water-soluble polyethylenimine as an efficient dispersant for gallium zinc oxide nanopowder in organic-based suspensions. Powder Technology. 2017;**305**:226-231

[4] Ahmad H, Lee CSJ, Ismail MA, Ali ZA, Reduan SA, Ruslan NE, et al. Zinc oxide (ZnO) nanoparticles as saturable absorber in passively Q-switched fiber laser. Optics Communications. 2016;**381**:72-76

[5] Nazarkovsky MA, Bogatyrov VM, Czech B, Galaburda MV, Wójcik G, Kolomys OF, et al. Synthesis and properties of zinc oxide photocatalyst by high-temperature processing of resorcinol-formaldehyde/zinc acetate mixture. Journal of Photochemistry and Photobiology A: Chemistry. 2017;**334**:36-46

[6] Pulit-Prociak J, Chwastowski J, Kucharski A, Banach M. Functionalization of textiles with silver and zinc oxide nanoparticles. Applied Surface Science. 2016;**385**:543-553

[7] Chen J, Zhang X, Cai H, Chen Z, Wang T, Jia L, et al. Osteogenic activity and antibacterial effect of zinc oxide/carboxylated graphene oxide nanocomposites: Preparation and in vitro evaluation. Colloids and Surfaces B: Biointerfaces. 2016;**147**:397-407

[8] Alswat AA, Ahmad MB, Saleh TA, Hussein MZB, Ibrahim NA. Effect of zinc oxide amounts on the properties and antibacterial activities of zeolite/zinc oxide nanocomposite. Materials Science and Engineering: C. 2016;**68**:505-511

[9] Gupta N, Grover R, Mehta DS, Saxena K. A simple technique for the fabrication of zinc oxide-PEDOT: PSS nanocomposite thin film for OLED application. Synthetic Metals. 2016;**221**:261-267

[10] Jia X, Wu N, Wei J, Zhang L, Luo Q, Bao Z, et al. A low-cost and low-temperature processable zinc oxide-polyethylenimine (ZnO:PEI) nano-composite as cathode buffer layer for organic and perovskite solar cells. Organic Electronics. 2016;**38**:150-157

[11] Bu IY-Y, Chen S. Improved crystalline silicon solar cells by light harvesting zinc oxide nanowire arrays. Optik: International Journal for Light and Electron Optics. 2016;**127**:10355-10359

[12] Mamat MH, Malek MF, Hafizah NN, Asiah MN, Suriani AB, Mohamed A, et al. Effect of oxygen flow rate on the ultraviolet sensing properties of zinc oxide nanocolumn arrays grown by radio frequency magnetron sputtering. Ceramics International. 2016;**42**:4107-4119

[13] Modaresinezhad E, Darbari S. Realization of a room-temperature/self-powered humidity sensor, based on ZnO nanosheets. Sensors and Actuators B: Chemical. 2016;**237**:358-366

[14] Ye Z, Wang T, Wu S, Ji X, Zhang Q. Na-doped ZnO nanorods fabricated by chemical vapor deposition and their optoelectrical properties. Journal of Alloys and Compounds. 2017;**690**:189-194

[15] Wang B, Duan Y, Zhang J. A controllable interface performance through varying ZnO nanowires dimensions on the carbon fibers. Applied Surface Science. 2016;**389**:96-102

[16] Zhou S-L, Zhang S, Liu F, Liu J-J, Xue J-J, Yang D-J, et al. ZnO nanoflowers photocatalysis of norfloxacin: Effect of triangular silver nanoplates and water matrix on degradation rates. Journal of Photochemistry and Photobiology A: Chemistry. 2016;**328**:97-104

[17] Schöttle C, Feldmann C. ZnO hollow nanospheres via Laux-like oxidation of Zn0 nanoparticles. Solid State Sciences. 2016;**55**:125-129

[18] Lin CJ, Liao S-J, Kao L-C, Liou SYH. Photoelectrocatalytic activity of a hydrothermally grown branched Zno nanorod-array electrode for paracetamol degradation. Journal of Hazardous Materials. 2015;**291**:9-17

[19] Dou Y, Wu F, Mao C, Fang L, Guo S, Zhou M. Enhanced photovoltaic performance of ZnO nanorod-based dye-sensitized solar cells by using Ga doped ZnO seed layer. Journal of Alloys and Compounds. 2015;**633**:408-414

[20] Ibrahim AA, Umar A, Kumar R, Kim SH, Bumajdad A, Baskoutas S. Sm_2O_3-doped ZnO beech fern hierarchical structures for nitroaniline chemical sensor. Ceramics International. 2016;**42**:16505-16511

[21] Bhatia S, Verma N, Bedi RK. Optical application of Er-doped ZnO nanoparticles for photodegradation of direct red-31 dye. Optical Materials. 2016;**62**:392-398

[22] Xu K, Liu C, Chen R, Fang X, Wu X, Liu J. Structural and room temperature ferromagnetic properties of Ni doped ZnO nanoparticles via low-temperature hydrothermal method. Physica B: Condensed Matter. 2016;**502**:155-159

[23] Manivannan A, Dutta P, Glaspell G, Seehra MS. Nature of magnetism in Co and Mn substituted ZnO prepared by sol-gel technique. British Journal of Applied Physics. 2006;**99**:08M110 (3 pages)

[24] Moditswe C, Muiva CM, Juma A. Highly conductive and transparent Ga-doped ZnO thin films deposited by chemical spray pyrolysis. Optik: International Journal for Light and Electron Optics. 2016;**127**:8317-8325

[25] Ismail AS, Mamat MH, Sin NDMd, Malek MF, Zoolfakar AS, Suriani AB, et al. "Fabri cation of hierarchical Sn-doped ZnO nanorod arrays through sonicated sol-gel immersion for room temperature, resistive-type humidity sensor applications. Ceramics International. 2016;**42**:9785-9795

[26] Dung ND, Son CT, Loc PV, Cuong NH, Kien PT, Huy PT, et al. Magnetic properties of sol-gel synthesized C-doped ZnO nanoparticles. Journal of Alloys and Compounds. 2016;**668**:87-90

[27] Ravichandran K, Dineshbabu N, Arun T, Manivasaham A, Sindhuja E. Synergistic effects of Mo and F doping on the quality factor of ZnO thin films prepared by a fully automated home-made nebulizer spray technique. Applied Surface Science. 2017;**392**:624-633

[28] Salah N, Hameed A, Aslam M, Abdel-wahab MS, Babkair SS, Bahabri FS. Flow controlled fabrication of N doped ZnO thin films and estimation of their performance for sunlight photocatalytic decontamination of water. Chemical Engineering Journal. 2016;**291**:115-127

[29] Meshram SP, Adhyapak PV, Amalnerkar DP, Mulla IS. Cu doped ZnO microballs as effective sunlight driven photocatalyst. Ceramics International. 2016;**42**:7482-7489

[30] Kim S-K, Gopi CVVM, Srinivasa Rao S, Punnoose D, Kim H-J. Highly efficient yttrium-doped ZnO nanorods for quantum dot-sensitized solar cells. Applied Surface Science. 2016;**365**:136-142

[31] Kim DH, Park J-H, Lee TI, Myoung J-M. Superhydrophobic Al-doped ZnO nanorods-based electrically conductive and self-cleanable antireflecting window layer for thin film solar cell. Solar Energy Materials and Solar Cells. 2016;**150**:65-70

[32] Meshki M, Behpour M, Masoum S. Application of Fe doped ZnO nanorods-based modified sensor for determination of sulfamethoxazole and sulfamethizole using chemometric methods in voltammetric studies. Journal of Electroanalytical Chemistry. 2015;**740**:1-7

[33] Anbia M, Fard SEM. Humidity sensing properties of Ce-doped nanoporous ZnO thin film prepared by sol-gel method. Journal of Rare Earths. 2012;**30**:38-42

[34] Peng X, Chu J, Yang B, Feng PX. Mn-doped zinc oxide nanopowders for humidity sensors. Sensors and Actuators B: Chemical. 2012;**174**:258-262

[35] Lee S-W, Choi BI, Kim JC, Woo S-B, Kim Y-G, Kwon S, et al. Sorption/desorption hysteresis of thin-film humidity sensors based on graphene oxide and its derivative. Sensors and Actuators B: Chemical. 2016;**237**:575-580

[36] Yao Y, Xue Y. Impedance analysis of quartz crystal microbalance humidity sensors based on nanodiamond/graphene oxide nanocomposite film. Sensors and Actuators B: Chemical. 2015;**211**:52-58

[37] Churenkov AV. Resonant micromechanical fiber optic sensor of relative humidity. Measurement. 2014;**55**:33-38

[38] Burgmair M, Zimmer M, Eisele I. Humidity and temperature compensation in work function gas sensor FETs. Sensors and Actuators B: Chemical. 2003;**93**:271-275

[39] Yao Y, Chen X, Li X, Chen X, Li N. Investigation of the stability of QCM humidity sensor using graphene oxide as sensing films. Sensors and Actuators B: Chemical. 2014;**191**:779-783

[40] Tang Y, Li Z, Ma J, Wang L, Yang J, Du B, et al. Highly sensitive surface acoustic wave (SAW) humidity sensors based on sol-gel SiO_2 films: Investigations on the sensing property and mechanism. Sensors and Actuators B: Chemical. 2015;**215**:283-291

[41] Ruiz V, Fernández I, Carrasco P, Cabañero G, Grande HJ, Herrán J. Graphene quantum dots as a novel sensing material for low-cost resistive and fast-response humidity sensors. Sensors and Actuators B: Chemical. 2015;**218**:73-77

[42] Hendi AA, Alorainy RH, Yakuphanoglu F. Humidity sensing characteristics of Sn doped Zinc oxide based quartz crystal microbalance sensors. Journal of Sol-Gel Science and Technology. 2014;**72**:559-564

[43] Zhao T, Fu Y, Zhao Y, Xing L, Xue X. Ga-doped ZnO nanowire nanogenerator as self-powered/active humidity sensor with high sensitivity and fast response. Journal of Alloys and Compounds. 2015;**648**:571-576

[44] Hsu N-F, Chang M, Hsu K-T. Rapid synthesis of ZnO dandelion-like nanostructures and their applications in humidity sensing and photocatalysis. Materials Science in Semiconductor Processing. 2014;**21**:200-205

[45] Hou J-L, Wu C-H, Hsueh T-J. Self-biased ZnO nanowire humidity sensor vertically integrated on triple junction solar cell. Sensors and Actuators B: Chemical. 2014;**197**:137-141

[46] Hong H-S, Chung G-S. Controllable growth of oriented ZnO nanorods using Ga-doped seed layers and surface acoustic wave humidity sensor. Sensors and Actuators B: Chemical. 2014;**195**:446-451

[47] Li Q, Liu X, Gu M, Huang S, Zhang J, Liu B, et al. Enhanced X-ray excited luminescence of Ga- and In-doped ZnO nanorods by hydrogen annealing. Materials Research Bulletin. 2017;**86**:173-177

[48] Son NT, Noh J-S, Park S. Role of ZnO thin film in the vertically aligned growth of ZnO nanorods by chemical bath deposition. Applied Surface Science. 2016;**379**:440-445

[49] Mamat MH, Sahdan MZ, Khusaimi Z, Ahmed AZ, Abdullah S, Rusop M. Influence of doping concentrations on the aluminum doped zinc oxide thin films properties for ultraviolet photoconductive sensor applications. Optical Materials. 2010;**32**:696-699

[50] Yue S, Wang L, Zhang D, Yang S, Guo X, Lu Y, et al. Facile synthesis of one-dimensional Fe-doped ZnO nanostructures from a single-source inorganic precursor. Materials Letters. 2014;**135**:107-109

[51] Malek MF, Mamat MH, Khusaimi Z, Sahdan MZ, Musa MZ, Zainun AR, et al. Sonicated sol–gel preparation of nanoparticulate ZnO thin films with various deposition speeds: The highly preferred c-axis (0 0 2) orientation enhances the final properties. Journal of Alloys and Compounds. 2014;**582**:12-21

[52] Malek MF, Mamat MH, Musa MZ, Soga T, Rahman SA, Alrokayan SAH, et al. Metamor phosis of strain/stress on optical band gap energy of ZAO thin films via manipulation of thermal annealing process. Journal of Luminescence. 2015;**160**:165-175

[53] Pascariu P, Airinei A, Olaru N, Petrila I, Nica V, Sacarescu L, et al. Microstructure, electrical and humidity sensor properties of electrospun NiO–SnO_2 nanofibers. Sensors and Actuators B: Chemical. 2016;**222:**1024-1031

[54] Khuili M, Fazouan N, El Makarim HA, El Halani G, Atmani EH. Comparative first principles study of ZnO doped with group III elements. Journal of Alloys and Compounds. 2016;**688**(Part B): 368-375

[55] Bai S, Guo T, Zhao Y, Sun J, Li D, Chen A, et al. Sensing performance and mechanism of Fe-doped ZnO microflowers. Sensors and Actuators B: Chemical. 2014;**195**:657-666

[56] Gao F, Liu XY, Zheng LY, Li MX, Bai YM, Xie J. Microstructure and optical properties of Fe-doped ZnO thin films prepared by DC magnetron sputtering. Journal of Crystal Growth. 2013;**371**:126-129

[57] Gürbüz O, Kurt İ, Çalışkan S, Güner S, Influence of Al concentration and annealing temperature on structural, optical, and electrical properties of Al co-doped ZnO thin films. Applied Surface Science. 2015;**349**:549-560

[58] Musat V, Teixeira B, Fortunato E, Monteiro RCC, Vilarinho P. Al-doped ZnO thin films by sol–gel method. Surface and Coatings Technology. 2004;**180-181:**659-662

[59] Wang W, Li Z, Liu L, Zhang H, Zheng W, Wang Y, et al. Humidity sensor based on LiCl-doped ZnO electrospun nanofibers. Sensors and Actuators B: Chemical. 2009;**141**:404-409

[60] Md Sin ND, Mamat MH, Malek MF, Rusop M. Fabrication of nanocubic ZnO/SnO_2 film-based humidity sensor with high sensitivity by ultrasonic-assisted solution growth method at different Zn:Sn precursor ratios. Applied Nanoscience. 2014;**4**:829-838

[61] Yang CC, Shen JY. Well-defined sensing property of ZnO:Al relative humidity sensor with selected buffer layer. Vacuum. 2015;**118**:118-124

[62] Zhu D, Hu T, Zhao Y, Zang W, Xing L, Xue X. High-performance self-powered/active humidity sensing of Fe-doped ZnO nanoarray nanogenerator. Sensors and Actuators B: Chemical. 2015;**213**:382-389

IntechOpen